– Supplementary Information –

"Discovery of Quasi-One-Dimensional Superconductivity in $PtPb_3Bi$"

Shashank Srivastava [1], Yash Vardhan,[2] Anshu Kataria,[1] Pradyumna Bawankule,[1] Poulami Manna,[1] Prabin Kumar Naik,[1] Rahul Verma,[2] Rhea Stewart,[3] James S. Lord,[3] Adrian D. Hillier,[3] Mathias S. Scheurer,[4] D. T. Adroja,[3,5] Bahadur Singh *,[2] and Ravi Prakash Singh * [1]

[1] *Department of Physics, Indian Institute of Science Education and Research Bhopal, Bhopal, 462066, India*

[2] *Department of Condensed Matter Physics and Materials Science, Tata Institute of Fundamental Research, Colaba, Mumbai 400005, India*

[3] *ISIS Facility, STFC Rutherford Appleton Laboratory, Oxfordshire, OX11 0QX, United Kingdom*

[4] *Institute for Theoretical Physics III, University of Stuttgart, 70550 Stuttgart, Germany*

[5] *Highly Correlated Matter Research Group, Physics Department, University of Johannesburg, Auckland Park 2006, South Africa*

* Corresponding emails: bahadur.singh@tifr.res.in, rpsingh@iiserb.ac.in

In the Supplementary Information, we present comprehensive details about experimental data on characterization, electrical transport, magnetization, specific heat, muon spin relaxation/rotation, electronic properties, and Uemura plot for $PtPb_3Bi$.

STRUCTURAL CHARACTERIZATION

The Rietveld refinement of the powder XRD pattern using $PtPb_3Bi$ crystallographic information file (CIF) is performed with FullProf Suite software. It confirms the phase purity and the tetragonal crystal structure under the space group $P4_2/mnm$ (No. 136, point group D_{4h}), which is nonsymmorphic and centrosymmetric in nature. The lattice constants obtained from the Rietveld refinement [$a = b = 11.4505(1)$ Å, $c = 4.0839(5)$ Å, $V_{cell} = 535.463(4)$ Å^3] agree well with the previously reported values [1, 2]. EDX analysis further confirms the nominal composition $Pt_{1.03}Pb_{3.08}Bi_{1.00}$ and homogeneity of the sample.

ELECTRICAL RESISTIVITY

The superconductivity in $PtPb_3Bi$ is confirmed by the zero-drop in resistivity at the transition temperature $T_{c,offset}$ of 3.08(1) K (inset of Fig. 1(b)). The transition temperature width of the zero-drop is 0.6 K, confirming the bulk superconductivity in the sample, supported by magnetization and specific heat measurements, discussed in the following sections.

Temperature variation of AC electrical resistivity $\rho(T)$ in the range of 1.9 K to 400 K under zero applied magnetic field was performed in both zero-field cooling and warming modes, and a clear bifurcation in the data is depicted in Figure 1(b). The difference in cooling and warming data indicates a charge density wave transition at $T_{CDW} = 280(1)$ K. The normal state resistivity data indicate a metallic behavior below T_{CDW}. The value of the residual resistivity ratio [RRR=ρ(400 K)/ρ(5 K)] is 1.19, indicating the presence of scattering and disorder in the sample [3].

MAGNETIZATION

The magnetization versus temperature measurement confirms the bulk superconductivity in $PtPb_3Bi$ compound. Magnetization was measured in the zero field-cooled warming (ZFCW) and the field-cooled cooling (FCC) modes under an applied field of 1 mT. The superconducting

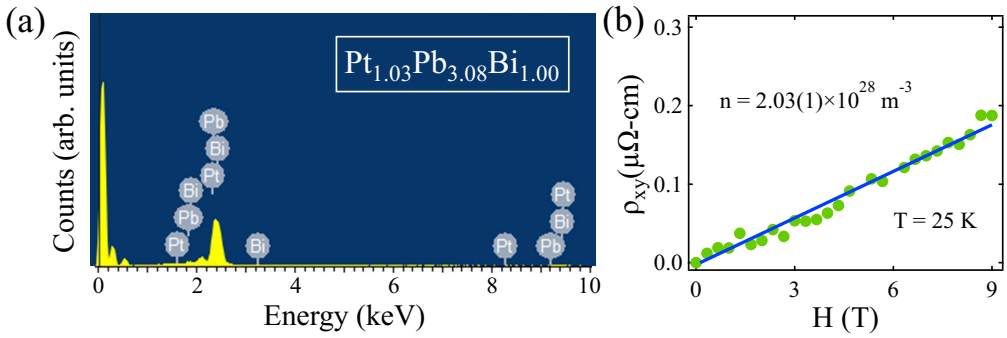

FIG. S1. (a) The EDX spectra for $PtPb_3Bi$ showing Pt, Pb and Bi elemental peaks. (b) The magnetic field variation of Hall resistivity at 25 K.

transition temperature obtained from the magnetization measurements is 3.01(1) K. A strong flux pinning can be observed from the separation of the FCC from the ZFCW curves, providing evidence of type II superconductivity. The superconducting volume fraction of ∼100% was calculated by incorporating the demagnetization factor (N) correction (depending on the shape of the sample and orientation with the applied magnetic field), as discussed in this section. The type II superconducting nature was affirmed by the magnetic field-dependent magnetization loop at 1.8 K, as illustrated in the inset of Figure 1(c), with irreversible magnetic field, $H_{irr} = 0.50(4)$ T.

Moreover, magnetization was measured under a low magnetic field range at different temperatures below T_C (refer to the inset of Fig. 1(d)). The lower critical field, H^*_{C1} values extracted at each temperature by the deviation of the curves from the Meissner line, give the lower critical fields at different temperatures. The slope of the Meissner line was used to calculate the demagnetization factor (N) using the relation $1/4\pi(1-N) = -M/H$ following ref. [4, 5]. Figure 1(d) describes the variation of H^*_{C1} with reduced temperature, which was fitted using the Ginzburg-Landau (GL) equation as,

$$H^*_{C1}(T) = H^*_{C1}(0)[1-t^2], \quad \text{where } t = \frac{T}{T_C}. \tag{1}$$

The intersection of the extrapolated fitting curve with the y-axis gives $H^*_{C1}(0) = 1.16(1)$ mT for $PtPb_3Bi$. The demagnetization corrected value of the lower critical field, $H_{C1}(0) = H^*_{C1}(0)/(1-N)$ was found to be 2.09(4) mT. Similarly, the values of the upper critical field, H_{C2} versus reduced temperature were also well fitted using the GL equation defined by Eq. 2 (refer to Fig. 1(e)). The values of H_{C2}(T) can be obtained from the temperature variation of both magnetization and resistivity data. Resistivity (and magnetization) curves show a decrease in T_C when the magnetic field is raised, providing the H_{C2} values at various temperatures (Fig.

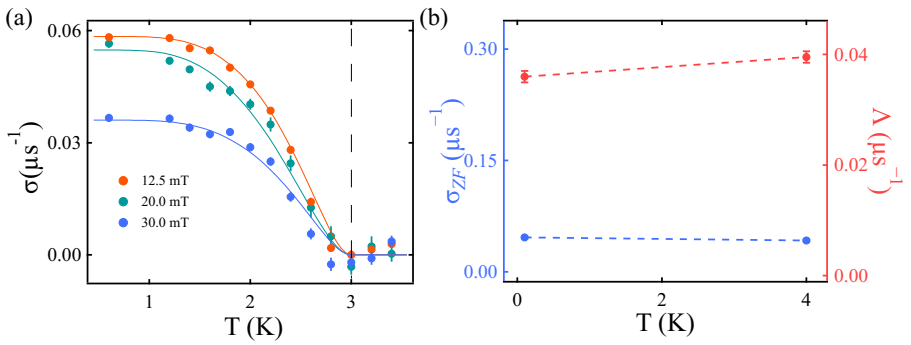

FIG. S2. (a) TF-μSR spin depolarization rate σ versus temperature T at applied magnetic fields from 12.5 to 30 mT. The dashed isothermal line separates the superconducting state and the normal state. The solid lines are a guide to the eye. (b) The unnoticeable changes in electronic relaxation rate Λ and nuclear relaxation rate σ_{ZF} with temperature within the error range.

1(e), inset).

$$H_{C2}(T) = H_{C2}(0)\left[\frac{1-t^2}{1+t^2}\right], \quad \text{where } t = \frac{T}{T_C}. \tag{2}$$

The extrapolation of the H_{C2}(T) versus T/T_C data gives an upper critical field $H_{C2}(0)$ value of 1.43(1) T and 1.32(1) T from the resistivity and magnetization measurements, respectively. $H_{C2}(0)$ value shows enhancement from the value of 0.35 T for the $PtPb_4$ compound [6].

Annihilation of superconductivity under the influence of a magnetic field can occur through two distinct mechanisms. (i) spin paramagnetic effect, a Cooper pair breaking caused by the Zeeman effect known as the Pauli limiting field $H^P_{C2}(0) = 1.86\ T_C$ [7, 8]. (ii) orbital limiting effect, caused by the increase in the kinetic energy of the supercurrent exceeding superconducting gap energy, which can be evaluated by the Werthamer-Helfand-Hohenberg (WHH) theory for a type-II superconductor using Eq. 3 [9, 10].

$$H^{orbital}_{C2}(0) = -\alpha T_C \left.\frac{dH_{C2}(T)}{dT}\right|_{T=T_C}, \tag{3}$$

where α is a constant called the purity factor, which has different values for dirty and clean limit superconductors (0.69 and 0.73, respectively). The value of $H^P_{C2}(0)$ for T_C of 3.01(1) K is 5.60(1) T, and $H^{orbital}_{C2}(0)$ was found to be 0.92(1) T for the dirty limit case. The value of $H_{C2}(0)$ is significantly lower than the Pauli paramagnetic limit of 5.60(1) T, signifying the role of orbital effects in the pair breaking. The impact of orbital effects can be quantified using the Maki parameter, $\alpha_m = \sqrt{2}\ \frac{H^{orbital}_{C2}(0)}{H^P_{C2}(0)}$, giving α_m of 0.23(2) for the limiting field values of the $PtPb_3Bi$ compound.

Characteristic length parameters, coherence length, ξ_{GL} and penetration depth λ_{GL} can be calculated using the relations $H_{C2}(0) = \frac{\phi_0}{2\pi\xi^2_{GL}(0)}$ and $H_{C1}(0) = \frac{\phi_0}{4\pi\lambda^2_{GL}(0)}\left[ln\frac{\lambda_{GL}(0)}{\xi_{GL}(0)} + 0.12\right]$, where ϕ_0 (magnetic flux quantum) is a constant [11]. The values of ξ_{GL} and λ_{GL} for the sample were

TABLE S1. Superconducting and normal state parameters extracted from magnetization, resistivity, specific heat, and μSR measurements for $PtPb_3Bi$.

Parameters	unit	$PtPb_3Bi$
T_C^{mag}	K	3.01(1)
$H_{C1}(0)$	mT	2.09(4)
$H_{C2}^{res}(0)$	T	1.43(1)
T_{CDW}	K	280(1)
ξ_{GL}	nm	15.8(1)
λ_{GL}^{mag}	nm	534.5(5)
κ_{GL}	-	33.8(4)
α_m	-	0.23(2)
γ_n	$mJmol^{-1}K^{-2}$	10.31(2)
θ_D^{sp}	K	128(1)
$\frac{\Delta(0)}{k_B T_C}$ (sp. heat)	-	2.03(1)
$\frac{\Delta(0)}{k_B T_C}$ (μSR)	-	2.27(4)
λ_{e-ph}	-	0.71(3)
$D_C(E_F)$	states/(eV f.u.)	4.37(2)
m^*/m_e	-	2.9(1)
n	10^{28} m^{-3}	2.03(1)
v_F	10^5 m/s	3.4(1)
ξ_0	nm	152.8(8)
l_e	nm	0.27(5)
μ_m	$cm^2V^{-1}s^{-1}$	0.35(1)
T_C/T_F	-	0.00028

calculated to be 15.8(1) nm and 534.5(5) nm, respectively.

The Ginzburg-Landau (GL) theory defined a parameter known as the GL parameter κ_{GL} to quantitatively distinguish between type-I and type-II superconductors. The value of $\kappa_{GL} = \frac{\lambda_{GL}(0)}{\xi_{GL}(0)}$ was estimated to be 33.8(4), which is much higher than $1/\sqrt{2}$, confirming that $PtPb_3Bi$ is a type-II superconductor. The thermodynamic critical field parameter H_C, can also be assessed using $H_{C1}(0)$ and $H_{C2}(0)$ [11]. Equation $H_C^2 ln\kappa_{GL} = H_{C1}(0)H_{C2}(0)$ gives $H_C = 28.0(2)$ mT. All superconducting characterization parameters estimated here are outlined in Table S1 for the $PtPb_3Bi$ compound.

SPECIFIC HEAT

Bulk superconductivity in the $PtPb_3Bi$ polycrystal is confirmed by using the temperature variation of specific heat $C(T)$ measurements. The significant jump in $C(T)/T$ versus T^2 in zero magnetic field manifests the superconducting transition temperature $T_C = 2.96(4)$ K of the sample (Fig. 1(f) inset). The $C(T)/T$ data above T_C is fitted using the Debye-Sommerfeld relation (Eq. 4). The first term $\gamma_n T$ represents the electronic contribution to the specific heat, and the following terms $\beta_3 T^3$ and $\beta_5 T^5$ denote the phononic and anharmonic contribution, respectively. The inset of Figure 1(f) shows the fitting of the low-temperature data with Eq. 4 yielding the Sommerfeld coefficient $\gamma_n = 10.31(2)$ mJmol^{-1}K^{-2}, the Debye constant $\beta_3 = 4.64(5)$ mJmol^{-1}K^{-4}, and $\beta_5 = 0.15(7)$ mJmol^{-1}K^{-6}.

$$C = \gamma_n T + \beta_3 T^3 + \beta_5 T^5. \tag{4}$$

The evaluated value of the density of state at the Fermi level $D_C(E_F)$ is 4.37(2) states eV^{-1}f.u.$^{-1}$ using the relation $\gamma_n = \left(\frac{\pi^2 k_B^2}{3}\right) D_C(E_F)$, where $k_B \simeq 1.38 \times 10^{-23}$ JK^{-1}. Debye temperature θ_D can be related to the Debye constant β_3 using the relation $\theta_D = \left(\frac{12\pi^4 RN}{5\beta_3}\right)^{\frac{1}{3}}$, and is calculated to be 127(8) K. The number of atoms per formula unit N is 5 for $PtPb_3Bi$ sample, and the universal gas constant R is taken as 8.314 Jmol^{-1}K^{-1}. The inverted McMillan's equation [12] can be used to calculate the electron-phonon coupling constant λ_{e-ph}, given as

$$\lambda_{e-ph} = \frac{\mu^* \ln(\theta_D/1.45T_C) + 1.04}{(1 - 0.62\mu^*)\ln(\theta_D/1.45T_C) - 1.04}; \tag{5}$$

where μ^* is a repulsive-screened Coulomb pseudopotential parameter that is taken to be 0.13 for intermetallic compounds. The value of λ_{e-ph} is 0.71(3) from the measured variables, indicating a moderate strength of electron-phonon coupling, which sustains superconductivity in the presence of a strong disordered quasi-1D material.

The variation of the normalized electronic specific heat with the reduced temperature was measured to analyze the nature of the superconducting gap symmetry of the sample. Electronic-specific heat C_{el} can be estimated by subtracting phononic and anharmonic contributions from the total specific heat C. The jump in normalized specific heat $\frac{\Delta C_{el}}{\gamma_n T_C}$ is 1.64(2), which is higher than the weak coupling limit from the BCS theory (i.e., 1.43). Further, Figure 1(f) shows the fitting of $C_{el}/\gamma_n T$ versus reduced temperature T/T_C with the isotropic single-gap BCS model given by Eq. 6 [13]. Models other than the s-wave model fail to properly describe the low-temperature specific heat behavior of $PtPb_3Bi$. The equation relates the entropy S_{el} to the temperature-dependent BCS energy gap $\Delta(t) = tanh[1.82\{1.018(\frac{1}{t} - 1)\}^{0.51}]$. The entropy S_{el} is

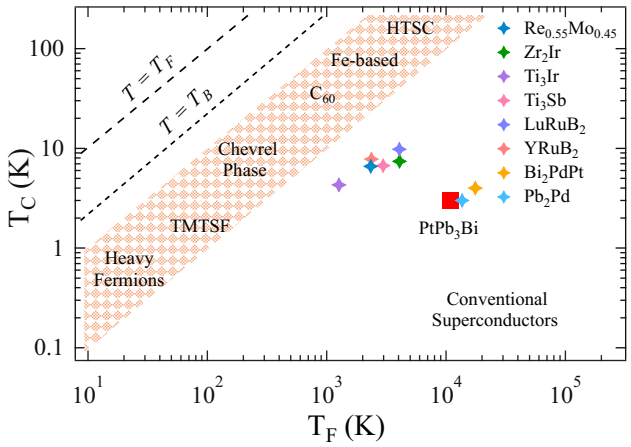

FIG. S3. The Uemura plot, superconducting critical temperature versus Fermi temperature, distinguishes the unconventional superconductors from the conventional BCS superconductors based on the ratio between T_C and T_F. The red square marker denotes $PtPb_3Bi$, which is away from the unconventional region.

related to C_{el} by $C_{el} = t\frac{dS_{el}}{dt}$, where $t = \frac{T}{T_C}$ is the reduced temperature.

$$\frac{S_{el}}{\gamma_n T_C} = -\frac{6}{\pi^2}\left(\frac{\Delta(0)}{k_B T_C}\right)\int_0^\infty [f_y ln(f_y) + (1-f_y)ln(1-f_y)]dy, \tag{6}$$

where the Fermi function $f_y(\xi) = [1 + e^{\frac{E(\xi)}{k_B T}}]^{-1}$ is integrated with respect to the Fermi energy $y = \xi/\Delta(0)$. The normal electron energy with respect to the Fermi energy is given as $E(\xi)=\sqrt{\xi^2 + \Delta^2(t)}$. The best fit of the normalized specific heat data results in a superconducting energy gap $\frac{\Delta(0)}{k_B T_C} = 2.03(1)$ that is higher than the weakly coupled BCS gap value of 1.76. The values of $\Delta C_{el}/\gamma_n T_C$ and $\Delta(0)/k_B T_C$ exceeding the BCS values indicate moderately coupled superconductivity in $PtPb_3Bi$.

TRANSVERSE-FIELD μSR

The TF μSR asymmetry spectra given in the main text were nicely fitted by the summation of sinusoidally oscillating functions, where each function is damped with a Gaussian relaxation component [14, 15]:

$$G(t) = \sum_{i=1}^{N} A_i \exp\left(-\frac{1}{2}\sigma_i^2 t^2\right)\cos(\gamma_\mu B_i t + \phi), \tag{7}$$

where ϕ, A_i, and σ_i are the initial phase, initial asymmetry, and the Gaussian relaxation rate, respectively. The value of the muon gyromagnetic ratio $\gamma_\mu/2\pi$ is 135.5 MHz/T, and B_i is the ith component of the Gaussian field distribution. The asymmetry spectra for the sample were

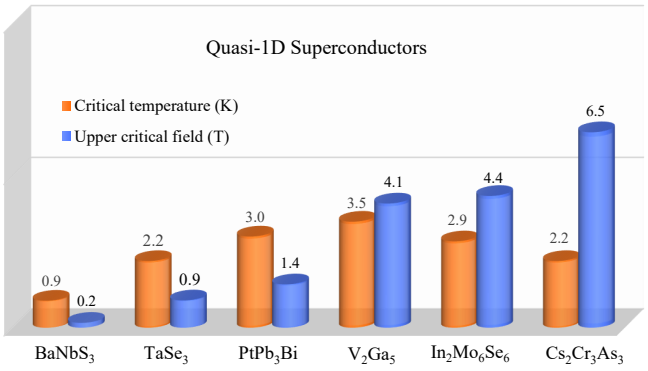

FIG. S4. Superconducting transition temperature and upper critical field of $PtPb_3Bi$, compared to some other quasi-1D superconductors [17–21].

best described by N = 2, representing two Gaussian components with fixed $\sigma_2 = 0$ to explain the non-depolarizing muon background stopped in the silver sample holder. Thus, A_2 (and B_2) account for the background asymmetry (and magnetic field), respectively.

The background nuclear dipolar contribution to the relaxation rate σ_N (considered to be temperature-independent for the temperatures discussed) can be removed from the total Gaussian relaxation rate σ_{total} to obtain the flux line lattice component of the Gaussian relaxation rate σ using equation $\sigma = \sqrt{\sigma_{total}^2 - {\sigma_N}^2}$. The deduced values of the superconducting contribution of the Gaussian relaxation rate σ(T) for different applied fields (12.5, 20, and 30 mT) are shown with the error bars in Figure S2(a). The field-dependent σ(H) at different temperatures is depicted in Figure 4(b), which was extracted from the isothermal values of σ(T) from Figure S2(a). Brandt's equation [16] described the field dependence of the penetration depth λ in an isotropic type II superconductor with $\kappa_{GL} > 5$ by Eq. 8, where $h = H/H_{C2}(T)$ is the reduced magnetic field.

$$\sigma(\mu s^{-1}) = 4.854 \times 10^4 (1-h)[1 + 1.21(1-\sqrt{h})^3]\lambda^{-2}. \quad (8)$$

This relation was used to fit the isothermal datasets in Figure 4(b) and extract the corresponding values of temperature-dependent λ^{-2}, which are presented in the main text, Figure 4(c).

ELECTRONIC PARAMETERS AND UEMURA PLOT

The normal state behavior of the charge carriers and the dependent electronic parameters were determined by performing Hall measurements on $PtPb_3Bi$. The data for Hall resistivity ρ_{xy} versus applied magnetic field is linearly fitted at 25 K, as shown in Figure S1(b). The slope of fitting provides the value of the Hall coefficient $R_H = 3.07(9) \times 10^{-8}$ ΩcmT^{-1}. The sign of R_H indicates holes as charge carriers with a concentration of $n = 1/eR_H = 2.03(1) \times 10^{28}$

m^{-3}. A superconductor can be designated to be in a clean or dirty limit based on the ratio of BCS coherence length $\xi_0 = 0.18\hbar v_F/k_B T_C$, and the mean free path $l_e = 3\pi^2\hbar^3/e^2\rho_0 m^{*2} v_F^2$ [11]. To calculate these parameters, the value of Fermi wave vector $k_F = (3\pi^2 n)^{1/3} = 8.4(3)$ nm^{-1}, effective mass $m^* = \gamma_n(\hbar k_F)^2/\pi^2 n k_B^2 = 2.9(1)m_e$ and Fermi velocity $v_F = \hbar(3\pi^2 n)^{1/3}/m^* = 3.4(1) \times 10^5$ ms^{-1} was evaluated using the value of γ_n and n from the specific heat and Hall measurement, respectively. The large value of the ratio between the parameters $\xi_0 = 152.8(8)$ nm and $l_e = 0.27(5)$ nm indicates dirty limit superconductivity likely due to imperfections and disorders. The value of the Ioffe–Regel parameter, $k_F l_e = 2.32(2)$, which is slightly above the Ioffe–Regel limit (~ 1), suggests a strongly disordered, diffusive metallic regime [22, 23]. Carrier mobility $\mu_m = 1/ne\rho$ can be calculated from the ρ and n from the resistivity and Hall measurements, respectively. The obtained value of $\mu_m = 0.35(1)$ cm^{2}V^{-1}s^{-1} is very low, placing the system in the dirty limit with diffusive normal state transport [23, 24].

Uemura et al. formulated a way to distinguish unconventional superconductors from conventional ones [25]. If the ratio of T_C and T_F is between 0.1 and 0.01, the superconductor is in the unconventional region, which is shown in Figure S3 with a highlighted band comprising notable unconventional superconductor families. The Fermi temperature $T_F = (3\hbar^3\pi^2 n)^{2/3}/2m^* k_B$ was calculated to be 10799(189) K [26]. The ratio of T_C and T_F for $PtPb_3Bi$ was found to be 0.00028, which lies out of the unconventional band and is shown with a red square marker. Some nonsymmorphic centrosymmetric compounds have been displayed for comparison purposes.

SUPPLEMENTARY REFERENCES

[1] Villars, P. *et al.* Structure types. part 10: Space groups (140)I4/mcm– (136)P42/mnm · $PtPb_3Bi$ (2011). Landolt-Börnstein - Group III Condensed Matter in SpringerMaterials (Springer-Verlag Berlin Heidelberg, 2011).

[2] Matković, T. & Schubert, K. Kristallstruktur von $PtPb_3Bi$. *J. Less-Common Met.* **59**, P35–P40 (1978).

[3] Grüner, G. The dynamics of charge-density waves. *Rev. Mod. Phys.* **60**, 1129–1181 (1988).

[4] Umezawa, A. *et al.* Anisotropy of the lower critical field, magnetic penetration depth, and equilibrium shielding current in single-crystal $YBa_2Cu_3O_{7-\delta}$. *Phys. Rev. B* **38**, 2843–2846 (1988).

[5] Carnicom, E. M. *et al.* $TaRh_2B_2$ and $NbRh_2B_2$: Superconductors with a chiral noncentrosymmetric crystal structure. *Sci. Adv.* **4**, eaar7969 (2018).

[6] Xu, C. Q. *et al.* Superconductivity in $PtPb_4$ with possible nontrivial band topology. *Phys. Rev. B* **104**, 125127 (2021).

[7] Chandrasekhar, B. S. A note on the maximum critical field of high-field superconductors. *Appl. Phys. Lett.* **1**, 7–8 (1962).

[8] Clogston, A. M. Upper limit for the Critical Field in Hard Superconductors. *Phys. Rev. Lett.* **9**, 266–267 (1962).

[9] Werthamer, N. R., Helfand, E. & Hohenberg, P. C. Temperature and Purity Dependence of the Superconducting Critical Field, H_{c2}. III. Electron Spin and Spin-Orbit Effects. *Phys. Rev.* **147**, 295–302 (1966).

[10] Helfand, E. & Werthamer, N. R. Temperature and Purity Dependence of the Superconducting Critical Field, H_{c2}. II. *Phys. Rev.* **147**, 288–294 (1966).

[11] Tinkham, M. *Introduction to superconductivity* (McGraw–Hill, New York, 1996), 2 edn.

[12] McMillan, W. L. Transition Temperature of Strong-Coupled Superconductors. *Phys. Rev.* **167**, 331–344 (1968).

[13] Padamsee, H., Neighbor, J. & Shiffman, C. Quasiparticle phenomenology for thermodynamics of strong-coupling superconductors. *J. Low Temp. Phys.* **12**, 387–411 (1973).

[14] Maisuradze, A., Khasanov, R., Shengelaya, A. & Keller, H. Comparison of different methods for analyzing μSR line shapes in the vortex state of type-II superconductors. *J. Phys.: Condens. Matter* **21**, 075701 (2009).

[15] Weber, M. *et al.* Magnetic-flux distribution and the magnetic penetration depth in superconducting polycrystalline $Bi_2Sr_2Ca_{1-x}Y_xCu_2O_{8+\delta}$ and $Bi_{2-x}Pb_xSr_2CaCu_2O_{8+\delta}$. *Phys. Rev. B* **48**, 13022–13036 (1993).

[16] Brandt, E. H. Properties of the ideal Ginzburg-Landau vortex lattice. *Phys. Rev. B* **68**, 054506 (2003).

[17] Tang, Z.-T. *et al.* Superconductivity in quasi-one-dimensional $Cs_2Cr_3As_3$ with large interchain distance. *Sci. China Mater.* **58**, 16–20 (2015).

[18] Petrović, A. P. *et al.* Phonon mode spectroscopy, electron-phonon coupling, and the metal-insulator transition in quasi-one-dimensional $M_2Mo_6Se_6$. *Phys. Rev. B* **82**, 235128 (2010).

[19] Neumeier, J. & Smith, M. Superconductivity in quasi-one-dimensional $BaNbS_3$. *Physica C* **542**, 1–5 (2017).

[20] Yamamoto, M. Superconducting properties of $TaSe_3$. *J. Phys. Soc. Jpn.* **45**, 431–438 (1978).

[21] Cheng, P.-Y. *et al.* Physical properties and electronic structure of the two-gap superconductor V_2Ga_5. *Phys. Rev. Res.* **6**, 033253 (2024).

[22] Ioffe, A. & Regel, A. Non-crystalline, amorphous, and liquid electronic semiconductors. *Prog.*

Semicond. **4**, 237 (1960).

[23] Lee, P. A. & Ramakrishnan, T. V. Disordered electronic systems. *Rev. Mod. Phys.* **57**, 287–337 (1985).

[24] Anderson, P. Theory of dirty superconductors. *J. Phys. Chem. Solids* **11**, 26–30 (1959).

[25] Uemura, Y. J. *et al.* Universal correlations between T_c and $\frac{n_s}{m^*}$ (carrier density over effective mass) in high-T_c cuprate superconductors. *Phys. Rev. Lett.* **62**, 2317–2320 (1989).

[26] Hillier, A. D. & Cywinski, R. The classification of superconductors using muon spin rotation. *Appl. Magn. Reson.* **13**, 95–109 (1997).